CELLO ANALYSIS OF SOLAR CELLS WITH SILICON OXIDE/SILICON NITRIDE REAR SIDE PASSIVATION: PARASITIC SHUNTING, SURFACE RECOMBINATION, AND SERIES RESISTANCE AS REAR SIDE INFLUENCES

A. Schütt[a)], J. Carstensen[a)], H. Föll[a)],
S. Keipert-Colberg[b)], and D. Borchert[b)]
[a)]: Institute for General Materials Science, Faculty of Engineering, Christian-Albrechts-University of Kiel,
Kaiserstr. 2, 24143 Kiel, Germany, email: jc@tf.uni-kiel.de, Phone: (+49) 431 880 6181, Fax: (+49) 431 880 6178
[b)]: Fraunhofer Institute for Solar Energy Systems, Laboratory and Servicecenter Gelsenkirchen,
Auf der Reihe 2, 45884 Gelsenkirchen, Germany

ABSTRACT: 120 µm thick multicrystalline Si solar cells with SiO/SiN stack rear-side passivation and Al point contacts are locally characterized using the CELLO technique. By combining different standard measurement modes—e.g. using different laser wavelengths, variation of global illumination intensity, and by measuring at different points along the *I-V* curve—effects due to parasitic shunting can be separated from other rear side effects like inhomogeneous surface passivation (i.e. due to stack or contacts) or series resistance. An increased series resistance at the rear side is found to improve the rear surface recombination behavior and thus induces a boost in the photocurrent response as an unexpected seemingly positive side effect. As a consequence the series resistance distribution of the rear side has to be taken into account for the correct interpretation of photocurrent data measured using light with long wavelengths.

Keywords: Characterization, Parasitic shunting, PERC

1 INTRODUCTION

It is well known that solar cells with rear side passivation need intensive process optimization with respect to the rear side passivation (influenced by e.g. doping, roughness, cleaning procedure etc.) and back contact formation (i.e. metallization co-firing and paste optimization for good ohmic contact and low surface recombination). It is also well known that rear side passivation concepts using a depletion layer might fall victim to parasitic shunting, i.e. the depletion layer becomes an inversion layer serving as a conducting layer with parasitic shunts, which in consequence enhances surface recombination by majority current recombination [1]. In this paper a systematic analysis of selected cells with rear side passivation by a SiO/SiN stack system [2] as presented in Fig. 1 is carried out using the CELLO technique.

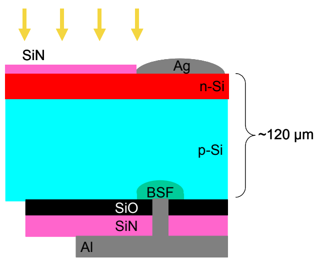

Fig. 1: Concept of characterized solar cell with rear side passivation by a SiO/SiN stack and Al point contacts.

2 THEORY

Fig. 2a) shows a standard equivalent circuit diagram of a solar cell with series resistance R_{SER}, parallel resistance R_P, photocurrent source I_{PH}, and the diode representing the p–n junction. For a linear small signal response measurement due to a modulated perturbation signal with angular frequency ω = $2\pi f$ the frequency dependence has to be taken into account as discussed in [3] by the equivalent circuit of Fig. 2b). For short-circuit condition R_D is large and can be neglected. The solar cells we investigate in this paper show no ohmic shunts so R_P can be neglected as well.

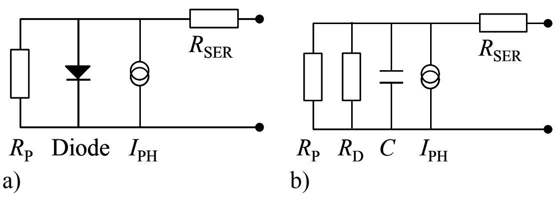

Fig. 2: Equivalent circuit models for describing solar cells: a) common one-diode model for large signals; b) corresponding linearization for small signal response analysis.

Therefore the frequency dependence of the short-circuit response signal—measured as amplitude $A_{x,y}$ and phase shift maps $\varphi_{x,y}$ by CELLO—is mainly given by a resistor and capacitor connected in parallel:

$$A_{x,y}\exp(i\varphi_{x,y}) = \frac{1}{1+i\omega R_{SER}C} + \dots \quad (1)$$

For a small phase shift φ this reduced to

$$\varphi(\omega) \approx \tan\varphi = \omega R_{SER}C + const. \quad (2)$$

with *const.* referring to additional phase shifts related to other transport processes in solar cells with typically a weaker frequency dependence, e.g. minority carrier diffusion. For local photocurrent measured at different frequencies $\omega_1 >> \omega_2$ in a good approximation the $R_{SER}C$ time constant can be separated from other time constants just by calculating

$$\varphi(\omega_1) - \varphi(\omega_2) = (\omega_1 - \omega_2)(R_{SER}C)_{x,y} \quad (3)$$

Since $(\omega_1 - \omega_2)$ is just a constant scaling factor Eq. (3) is a very convenient way to map local inhomogeneities of $R_{SER}C$. Thus a local change of $R_{SER}C$—e.g. when changing the global illumination—can be analyzed by

$$(\omega_1 - \omega_2)\left[R_{SER}C_{x,y}^{\text{illuminatd}} - R_{SER}C_{x,y}^{\text{dark}}\right] = (\omega_1 - \omega_2)\Delta(R_{SER}C)_{x,y} \quad (4)$$

3 EXPERIMENTAL

3.1 Samples

Several 150 µm thick multicrystalline Si wafers undergo an industrial-like cell process sequence [2] for the cell concept as shown in Fig. 1. Diffusion and PSG removal is followed by back-etching of the parasitic emitter by removing 3–6 µm on the rear side. Then both cell sides are chemically cleaned and ARC-SiN is deposited on the front and a SiO/SiN stack is deposited on the back side for rear side passivation by PECVD. Contact holes in the stack are opened by a photolithography step with subsequent etching. By screen printing opened holes are filled with Al paste establishing after co-firing an ohmic contact and surface passivation by an Al-BSF. The final thickness of the cell after all etching and cleaning steps is around 120 µm.

3.2 Measurements

In CELLO measurements a sinusoidally intensity modulated laser beam is scanned across the solar cell and the response signal (containing amplitude and phase shift φ information) is recorded as photocurrent maps dI_x (x = SC: potentiostatic at short-circuit condition, x = MPP: potentiostatic at maximum power point) [4]. For this analysis a series of experiments was conducted with various laser wavelengths (RED = 658 nm, IR = 830 nm, SIR = 934 nm), with differing global illumination conditions using white halogen bias light, and with higher spatial resolution scans.

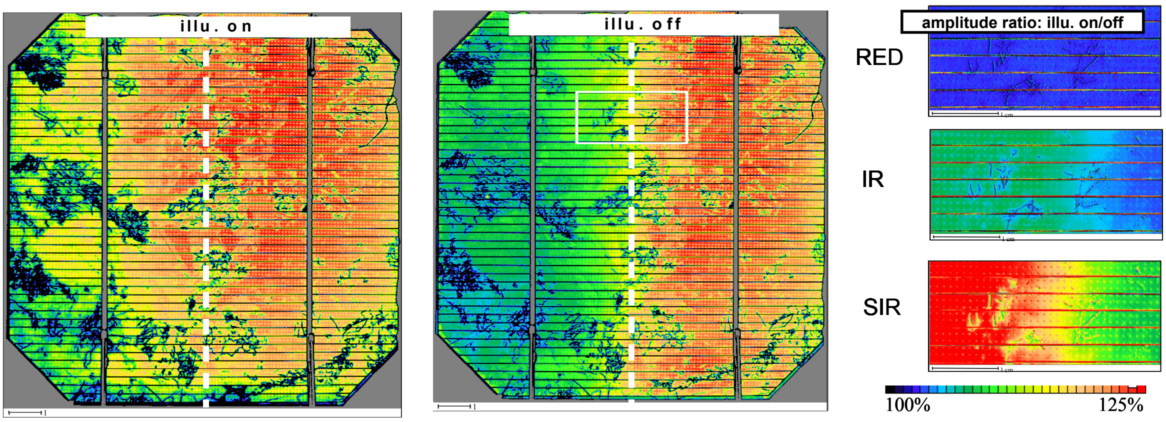

a) b) c)

Fig. 3: dI_{SC} amplitude maps of SIR laser (934 nm) with identical scale and a) 1/3 sun global illumination (i.e. illu. on) and b) zero global illumination (i.e. illu. off). High values in the maps are presented in red, low values in blue, so strong photocurrent losses on the left side of the cell are visible in b); c) amplitude ratio maps for global illumination on/off of the selected area marked in b), equally scaled, for different lasers (RED = 658 nm, IR = 830 nm, SIR = 934 nm), showing that the losses on the left side become stronger with longer laser light wavelengths.

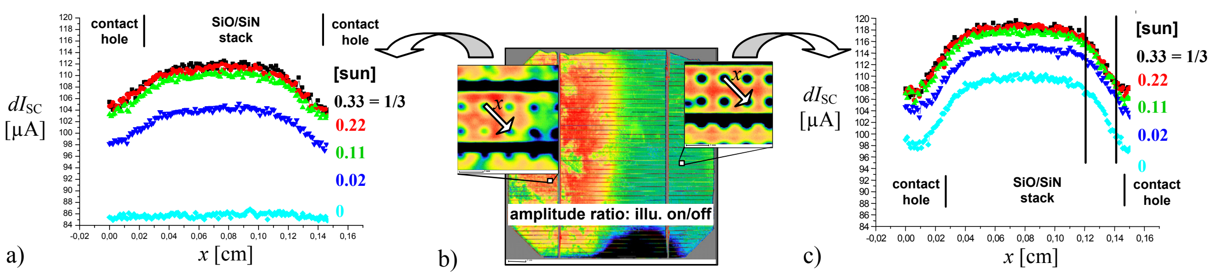

Fig. 4: Al-contact to Al-contact line scans with high spatial resolution (120 pixel per mm) of dI_{SC} maps using the SIR laser (934 nm) for various global illumination intensities (1/3 sun to 0 sun). a) Line scans in an area with losses in Fig. 1b); b) SIR overview map in where white arrows indicate the path of the line scan in two high spatial resolution map; c) line scans in a normal area without losses in Fig. 1b). Comparing the line scans the photocurrent response is always larger in the normal area. Higher global illumination increases the photocurrent response in both areas. In the defected area (left) the line scan without global illumination shows a constant response (i.e. parasitic shunting as described in the text) while in all other line scans a plateau of high photocurrent is visible (lower S_{back} due to SiO/SiN stack) adjacent to the reduced photocurrent areas of the point contacts (higher S_{back} due to Al-BSF).

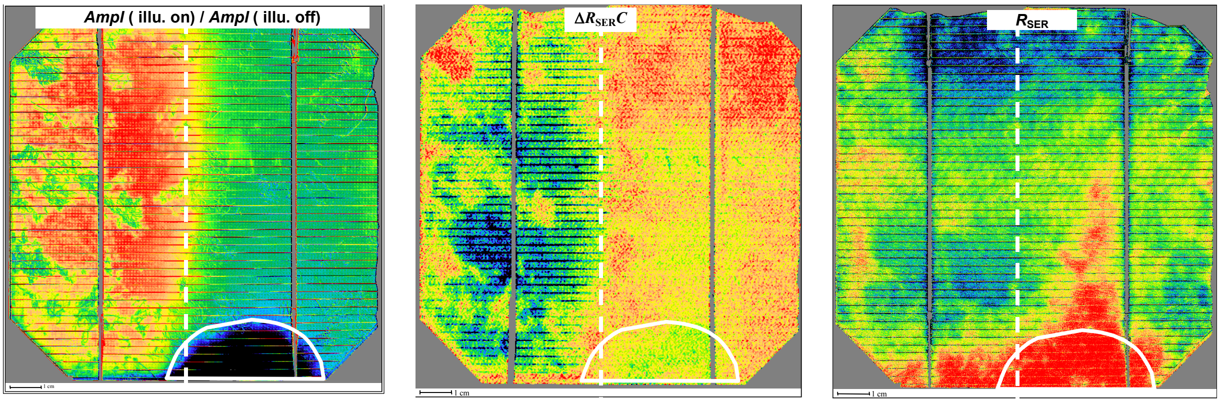

a) b) c)

Fig. 5: Maps from various SIR laser (934 nm) measurements (color scheme for representation of values as in Fig. 3): a) amplitude ratio map (i.e. global illumination on/off); b) difference map calculated according to Eq. (4) visualizing $\Delta R_{SER}C$ due to change of global illumination; c) standard CELLO R_{SER} map [4]. Despite an offset (change of scaling factor) at the dashed line a good agreement is found between b) and c) indicating that in the areas left and right of the dashed line mainly ΔC changes when the global illumination changes. There is good correlation between a) and b), the white semicircle indicates expected deviations due to a very high series resistance at the front contact.

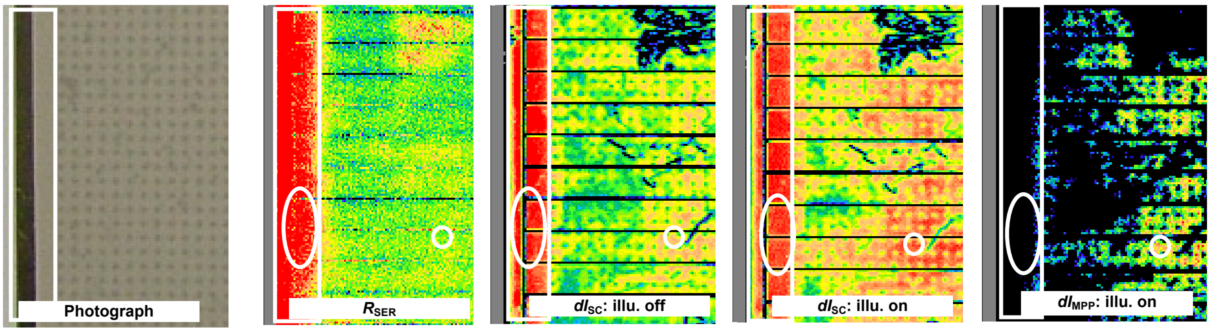

a) b) c) d) e)

Fig. 6: a) The photograph of the rear side (mirrored for easier comparison) shows an area (white rectangle) with missing contact holes (elsewhere visible as dark dots) and thus increased series resistance. As expected this area shows up in the R_{SER} map presented in b) (red color means high R_{SER}). The short-circuit current dI_{SC} maps using the SIR laser (934 nm) without c) and with d) global illumination show a large photocurrent (red color) for that area. e) The map of the photocurrent at maximum power point dI_{MPP} using the SIR laser with global illumination allows to distinguish between increased R_{SER} and improved passivation (see circles) just from a current map.

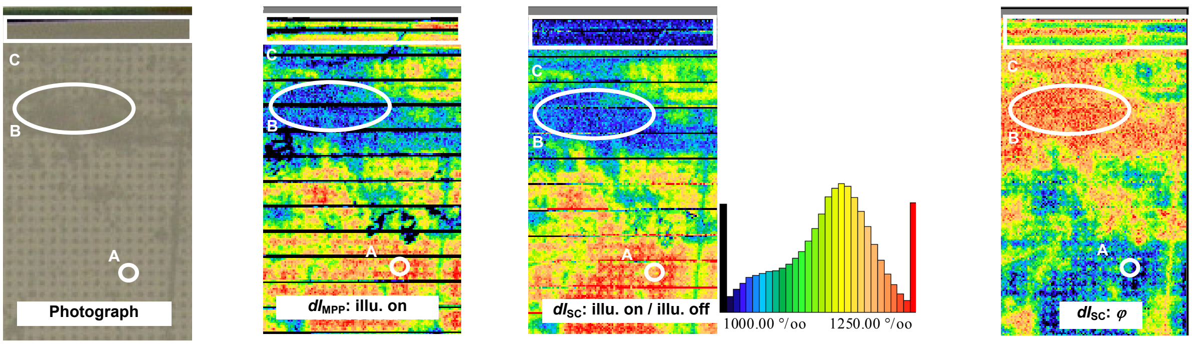

a) b) c) d)

Fig. 7: a) Photograph of the rear side (mirrored for easier comparison); b)–d) maps taken using the SIR laser (934 nm): b) photocurrent at maximum power point dI_{MPP} with 1/3 sun global illumination (color scheme as before); c) illu. on/off ratio of short-circuit current dI_{SC} maps; d) phase shift of the short-circuit photocurrent with illu. on. The highlighted (white mark) dark-grey areas in a) visualize areas around the edge of the cell (C) or having defects in the lithography mask (B) and thus are places where Al rear contact formation took place on large areas (i.e. not limited to point contacts; A).

4 RESULTS AND DISCUSSION

4.1 Photocurrent losses due to parasitic shunting

The CELLO setup allows to control the global illumination intensity using white light in the range of 1/3 sun (abbreviation: illu. on) to 0 suns (abbreviation: illu. off). The results in Fig. 3 are obtained from dI_{SC} measurements with 1/3 and 0 sun global illumination for laser light of various wavelengths. The SIR (934 nm) laser map of 0 sun in Fig. 3b) in comparison with the 1/3 sun map in Fig. 3a) shows strong losses on the left side of the cell. These losses are only visible when switching off the global illumination. This is a well-known effect for cells showing parasitic shunting [1]. Parasitic shunting means the existence of an inversion layer which allows an easy lateral current flow to regions that strongly shunt the photo-generated charges. For the cell investigated here with p-type bulk material a thin conductive n-type layer exists which allows an easy transport of electrons to the point contacts where the shunting by recombination with holes takes place. This mechanism increases the local losses of minority carriers at the back side of the solar cell and thus S_{back}.

It is well known that the inversion layer can be influenced e.g. by additional global illumination. To check for the validity of this parasitic shunting model in our solar cell and to learn more about the interaction of local charge carrier density and local lateral transport, in what follows CELLO measurements under various global illumination conditions are combined.

In the area marked by the white rectangle in Fig. 3b) high resolution short-circuit current dI_{SC} measurements using three laser with different wavelengths (RED, IR, and SIR) have been performed with and without additional global illumination (1/3 and 0 sun). For each wavelength the amplitude ratio is calculated by dividing the map taken under illumination by the map taken in the dark; these ratio maps are presented in Fig. 3c) with an identical scale. The photocurrent gain due to 1/3 sun global illumination is strongest for the deeply penetrating SIR laser (around 30%), which is a strong indication that, as expected, the gain in photocurrent due to additional global illumination is mainly related to changes in the losses at the back surface of the solar cell.

For the same cell SIR laser short-circuit current dI_{SC} line-scans with extremely high spatial resolution (120 pixel per mm) and various global illumination intensities are presented in Fig. 4. The locations of the two line scan positions used for the scans in Fig. 4a) and 4c) are presented in Fig. 4b). Both line scan positions are located in homogeneous grains so that no bulk recombination influences the measurement.

The line scans in Fig. 4c) represent the data in the non-defected area. When changing the global illumination the shape of these curves does not change; just an offset occurs. A plateau of high photocurrents is found in the central part far away from the contact holes. Strongly reduced photocurrents are found at the contact holes with a transition regime of roughly 200 µm width indicated by the two vertical lines in Fig. 4c). This is expected for this rear side passivation concept because the rear surface recombination velocity S_{back} at the area with dielectric stack passivation is smaller than at the Al-BSF contact area. The transition regime width of 200 µm can be well interpreted as an effective diffusion length for the diffusion of minority carriers to the point contact areas. The improvement of back surface passivation by additional global illumination is typical for floating junction passivation, as obtained e.g. by a dielectric stack of SiO/SiN.

A completely different result is found for the line scans across the defected area in Fig. 4a). Without global illumination the photocurrent is drastically decreased to a nearly constant value for the contact holes as well as for the passivation stack area. This flat curve is a first strong hint that the transport of minority carriers from the dielectric-stack-passivated areas to the contact holes becomes much easier. The length scale is too large for a diffusion process of minority carriers. Successively increasing the global illumination a plateau shows up as in the case of Fig. 4c), but the transition regime is always wider and the photocurrent losses are always larger than in the non-defected region.

4.2 $R_{SER}C$ effects due to parasitic shunting

Fig. 5a) presents the map of Fig. 3a) divided by the map of Fig. 3b) that nicely visualizes the parasitic shunted areas (red color). From the phase shift maps that correspond to Fig. 3a) and b) and two additional phase shift maps using higher frequencies (all not shown) a phase shift difference obtained according to Eq. (4) is shown in Fig. 5b). The standard CELLO series resistance map R_{SER} [4] is shown in Fig. 5c). Clearly the difference between the left and the right side separated by the dashed line is visible in Fig. 5a) and 5b) but not in Fig. 5c). Additionally several features visible in the series resistance map show up in Fig. 5b) as well. Both results can be easily understood by stating that the main difference between switching on and off the global illumination is a significant change in capacitance ΔC on the defected left side of the solar cell. Again this result is in good agreement with the existence of an inversion layer with a capacitance ΔC which vanishes when globally illuminating the cell.

As simple as the explanation of an inversion layer seems, there is a problem: Why does the laser light not lead to a vanishing of the inversion layer like the global illumination does—especially since the laser illumination induces a current density roughly one order of magnitude larger than the homogeneous illumination? The answer is related to the illumination being inhomogeneous. The local voltage drop ΔU needed to close the inversion channel is related to the voltage drop across the inversion layer far away from the illuminated spot and the ohmic losses induced by the current flow away from the illuminated spot as shown schematically in Fig. 8.

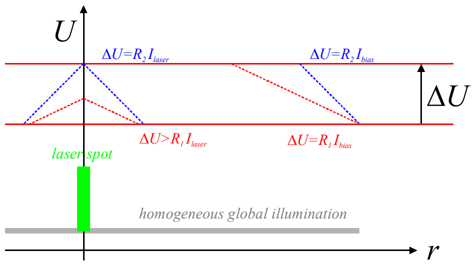

Fig. 8: Schematic of inversion-layer closing condition for different channel resistances ($R_1 < R_2$) and for different currents ($I_{laser} << I_{bias}$). Only with R_1 and I_{laser} the channel is not closed.

For a given channel resistance R_{channel} the laser-generated photocurrent I_{laser} must be large enough to induce an ohmic loss

$$R_{\text{channel}} I_{\text{laser}} > \Delta U \quad . \tag{5}$$

Obviously for the SIR laser this condition is not fulfilled for the left side of the solar cell. Still the condition of Eq. (5) can be easily checked in many areas on the defected left side of the solar cell. Fig. 6 summarizes CELLO maps near the edge of the cell where point contacts are missing. Correspondingly the series resistance is large close to the edge (cf. Fig. 6b). In this region the short-circuit photocurrent is much larger than in the neighboring areas with point contacts; no significant differences are found with and without illumination. This result can be understood by Eq. (5) taking into account the strongly increased ohmic losses $R_{\text{channel2}} > R_{\text{channel1}}$ due to the point contacts being located far away from the laser illuminated spot. Now the laser current probably is large enough to fulfill Eq. (5).

In a last set of experiments the validity of Eq. (5) has been tested by reducing the current of the global illumination successively. Using a mask, only square areas around the laser spot were illuminated with 1/3 sun intensity of homogeneous white light. When reducing the size of the illuminated area below 2 mm^2 parasitic shunting became visible again. This second condition for the global illumination necessary for closing the inversion channel is illustrated in Fig. 8 as well. Up to now it is not clear on which length scale lateral ohmic losses have to be taken into account, i.e. only to the nearest point contacts or across the back side metallization into non-illuminated parts further away.

Like in this CELLO example, limiting the area of global illumination to small sizes may lead to parasitic shunting and thus might be misinterpreted as an area with increased S_{back}. This is important e.g. for the correct interpretation of results obtained from measurements using larger wavelengths in combination with small illuminated areas (e.g. IQE or reflectivity measurements that use partial area illumination).

Table I: Al rear contact classification

label	mask opened by	mark	map color of Fig. 7b)	map color of Fig. 7c)
A	point	circle	yellow	yellow
B	damage	ellipse	yellow	blue
C	area	rectangle	blue	blue

Just to make sure that not the areas with Al-BSF are the reason for the strong dependence of the short-circuit photocurrent on the globally illuminated cell, Fig. 7 is presented. Three different areas with Al-BSF are distinguished as summarized in Table I. Especially the edge area C does not show any dependence on global illumination as may be expected for Al-BSF backside passivation. For A, B, and C the CELLO R_{SER} map (not presented here) is very homogeneous but the phase shift map of dI_{SC} with full global illumination in Fig. 7d) is exactly inverse to Fig. 7b), i.e. only area B has very small phase shift, which is a typical indicator for increased recombination. So the power losses in area B most probably are caused by increased S_{back} due to a not optimal Al-BSF formation process at this location.

The discussion and interpretation of the back surface properties of the solar cell in Fig. 4 and 5 was so easy because there was this clear difference between left and right side of the cell. Only one fabrication step could be identified which may explain the nearly perfect vertical separation line: a very short (12 seconds) back etching step for removing the parasitic emitter from the back side of the cell by dipping into CPX4. This has been done manually and any delay may lead to an imperfect removal of the highly doped layer in the left part of the cell. After several cleaning steps the back side of the cell is coated with the stack of dielectric layers. If this explanation is right, remains of the highly doped n-layer would exist below the dielectric stack acting as an n-channel in the same way as an inversion channel induced by charges in the dielectric stack.

5 CONCLUSION

For solar cells with parasitic shunting various measuring conditions of the CELLO system (various laser wavelengths, various spatial resolutions, and various intensity levels of global bias illuminations) allow a systematic study of parasitic shunting on photocurrent measurements. Strong effects of parasitic shunting due to local and global illumination intensity and due to local series resistance distribution are explained by a simple model that introduces a closing condition for the inversion layer that leads to parasitic shunting. As a consequence for the correct interpretation of photocurrent measurements—especially for the wavelengths crucial for determining S_{back}—it is necessary to also take into account the local lateral series resistance as well as the distribution and magnitude of local and/or global photocurrents. It is demonstrated that a combination of typical CELLO measurements separates local losses caused by parasitic shunting from others like e.g. reduced rear side passivation (increased S_{back}) or rear side series resistance, allowing to identify limiting process steps and thus a more specific cell optimization process for solar cells with rear side passivation.

6 ACKNOWLEDGEMENTS

This work was supported by the Deutsche Forschungsgemeinschaft under contract No. FO 285/11-2.

7 REFERENCES

[1] I. Cesar, E. Bende, G. Garibiati, L. Janssen, A. Weeber, and J. Bultmann, in Proceedings, 34th IEEE Photovoltaic Specialists Conference, Philadelphia, USA (7-12 June 2009).

[2] S. Keipert-Colberg, N. Barkmann, C. Streich, A. Schütt, D. Suwito, P. Schäfer, S. Müller, and D. Borchert, in Proc. 26th European Photovoltaic Solar Energy Conference, 2BV.3.61, Hamburg (2011).

[3] J. Carstensen, A. Schütt, A. Pape, and H. Föll, in Proc. 25th European Photovoltaic Solar Energy Conference, 2CV.3.19, Valencia (2010).

[4] A. Schütt, J. Carstensen, H. Föll, S. Keipert-Colberg, and D. Borchert, in Proc. 26th European Photovoltaic Solar Energy Conference, 2BV.2.39, Hamburg (2011).